Etching-induced damage in heavily Mg-doped p-type GaN and its suppression by low-bias-power inductively coupled plasma–reactive ion etching

Takeru Kumabe[1]*, Yuto Ando[1], Hirotaka Watanabe[2], Manato Deki[1,3], Atsushi Tanaka[2,4], Shugo Nitta[2], Yoshio Honda[2], and Hiroshi Amano[2,3,4,5]

[1]*Department of Electronics, Nagoya University, Nagoya, Aichi 464-8603, Japan*

[2]*Institute of Materials and Systems for Sustainability, Nagoya University, Nagoya, Aichi 464-8601, Japan*

[3]*Venture Business Laboratory, Nagoya University, Nagoya, Aichi 464-8601, Japan*

[4]*National Institute for Materials Science, Tsukuba, Ibaraki 987-6543, Japan*

[5]*Akasaki Research Center, Nagoya University, Nagoya, Aichi 464-8603, Japan*

E-mail: kumabe@nagoya-u.jp

Inductively coupled plasma–reactive ion etching (ICP–RIE)-induced damage in heavily Mg-doped p-type GaN ([Mg] = 2×10^{19} cm^{-3}) was investigated by low-temperature photoluminescence (PL) and depth-resolved cathodoluminescence (CL) spectroscopy. From PL measurements, we found broad yellow luminescence (YL) with a maximum at around 2.2–2.3 eV, whose origin was considered to be isolated nitrogen vacancies (V_N), only in etched samples. The depth-resolved CL spectroscopy revealed that the etching-induced YL was distributed up to the electron-beam penetration depth of around 200 nm at a high ICP–RIE bias power (P_{bias}). Low-bias-power (low-P_{bias}) ICP–RIE suppressed the YL and its depth distribution to levels similar to those of an unetched sample, and a current–voltage characteristic comparable to that of an unetched sample was obtained for a sample etched with P_{bias} of 2.5 W.

1. Introduction

GaN plays an important role in high-power and high-frequency semiconductor devices. In recent years, GaN-based vertical trench-gate metal–oxide–semiconductor field-effect transistors (MOSFETs) with a high breakdown voltage of > 1 kV and a low specific on-resistance of 1.8 mΩ cm^2 have been demonstrated and are in the spotlight[1,2]. On the other hand, GaN-based heterojunction bipolar transistors (HBTs) are also attracting attention for their power handling capability, normally-off and expected high-frequency characteristics[3,4]. Since GaN is a chemically resistant material[5], dry etching techniques including inductively coupled plasma–reactive ion etching (ICP–RIE) are widely used in device fabrication processes. However, it is well known that ion bombardment in the dry etching processes results in the formation of nitrogen vacancy (V_N)-related defect levels[6,7], which degrade material and device characteristics[8,9]. Therefore, reducing etching-induced damage is highly desired for the development of GaN-based devices.

Various studies on dry etching techniques and post–dry-etching treatments have been carried out towards the suppression of the damage in GaN. Looking first at dry etching techniques, effects of a high stage temperature[10,11] and plasma conditions[12,13] on the damage have been investigated. As for postetching treatments, the wet etching removal of a damaged layer[14], damage recovery utilizing N_2 plasma exposure[15,16] or NH_3/N_2 annealing[17-19], and a combination of these methods[20] have been reported. Although these methods resulted in improved electrical properties of an etched GaN film compared with those without any treatment, it is difficult to recover the characteristics to those before etching. Recently, it has been reported that ICP–RIE with two- or multistep bias power (P_{bias}) including an ultralow P_{bias} combined with thermal annealing significantly suppressed the damage formed in n-type GaN[21,22], and Schottky characteristics similar to those of an unetched sample were demonstrated[22]. It is also essential for the fabrication of high-performance GaN-based vertical trench-gate MOSFETs and HBTs to suppress etching-induced damage in p-type GaN; however, a low-damage dry etching technique for p-type GaN has not yet been established. Moreover, there is little information on the damage in heavily Mg-doped p-type GaN.

In this study, we investigated etching-induced damage in heavily Mg-doped p-type GaN by low-temperature photoluminescence (PL) and depth-resolved cathodoluminescence (CL) spectroscopy. In addition, low-P_{bias} ICP–RIE was carried out to suppress the damage and improve the electrical properties. Compared with the previous study[23], the distribution of the damage was newly investigated by depth-resolved CL spectroscopy.

2. Experimental methods

Sample preparation started with the growth of a 1-μm-thick heavily Mg-doped p-type GaN layer ([Mg] = 2×10^{19} cm^{-3}) on a *c*-plane Si-doped n-type free-standing GaN substrate by metal organic vapor phase epitaxy. Fig. 1 shows the schematic process flow of surface etching and electrode formation. After cleaning by the standard RCA procedure[24], the entire surface of each sample was etched to 300±10 nm by ICP–RIE (Samco RIE-200iP-NXT). In the etching process, Cl_2 was employed as reactive gas with its flow rate and pressure kept at 30 sccm and 2.0 Pa, respectively. ICP antenna power was maintained at 150 W and P_{bias} was set at 2.5, 5.0, 15, and 30 W for each sample within an error of ±0.3 W. The corresponding etching time was considered to be 1605, 428.5, 150, and 75.6 s, respectively. Afterward, the samples were annealed at 973 K in N_2 atmosphere for 5 min by rapid thermal annealing (RTA) so as to activate Mg acceptors.

Low-temperature PL and depth-resolved CL spectroscopy were performed to evaluate the etching-induced damage and its distribution in the depth direction. PL measurements were carried out using a continuous-wave diode-pumped solid-state laser with a photon energy of 3.875 eV under a weak excitation of 4 W/cm^2. The temperature of the sample stage was controlled in the range of 5–200 K, and spectra were measured using an Ocean Optics FLAME-S UV–VIS spectrometer. Depth-resolved CL measurements were performed using a GATAN MonoCL system installed on a Hitachi S4300 field-emission scanning electron microscopy (SEM) device. The CL signal was dispersed using a 1200 lines/mm grating brazed at 500 nm and detected using a Peltier-cooled photomultiplier tube. Electron-beam energy (E_b) was varied from 3.0 to 10.0 keV to investigate depth-resolved luminescence properties of the samples down to depths of around 700 nm. Electron-beam current (I_b) was also modified while monitoring its value using a Faraday cup to control electron-beam power ($P_b = E_b \times I_b$).

To evaluate electrical contacts on the etched surfaces, Ni/Au metal stacked electrodes were formed on the samples. A 20-nm-thick Ni layer and a 100-nm-thick Au layer were deposited by electron-beam evaporation and alloyed at 798 K in O_2 atmosphere for 5 min by RTA. Subsequently, current–voltage (*I–V*) measurement was carried out using a Keysight B1500A semiconductor parameter analyzer.

3. Results and discussion

Fig. 2 shows the low-temperature PL spectra of (a) unetched p-type GaN and (b) p-type GaN

etched by ICP–RIE with P_{bias} of 15 W. Two or three sets of PL bands can be seen for each sample. The first set is an ultraviolet luminescence (UVL) band with a main peak at around 3.29 eV. The main peak originates from the transition of a shallow donor or the conduction band minimum to a Mg acceptor substituted in a Ga site (Mg_{Ga})[25], where the following peaks at 3.20, 3.10, and 3.02 eV are its LO phonon replicas[25]. The second set is a blue luminescence (BL) band with a peak at around 2.6 eV. This luminescence is unique to heavily Mg-doped GaN, and its origin is the transition of a deep donor to a Mg_{Ga} acceptor[25]. The final set is a yellow luminescence (YL) band with a maximum at around 2.2–2.3 eV, which was only seen in the etched samples. Kato *et al*. investigated deep levels in n-type GaN etched under conditions similar to those used in this study by deep-level transient spectroscopy (DLTS). They observed an increase in the concentration of donor-type defects with an activation energy of 0.25 eV and concluded its origin to be V_N[21]. Yan *et al*. studied the effects of V_N on electrical and optical properties of Mg-doped GaN using hybrid functional calculations. They reported that the isolated V_N acts as a compensation center with a 3+ charge state in Mg-doped p-type GaN and gives rise to a PL peak at 2.18 eV[26]. Therefore, the ICP–RIE-induced V_N is a plausible candidate for the origin of YL.

In addition, it was observed that the YL-to-UVL ratio varied with P_{bias}. The dependence of the ratio on P_{bias} is shown in Fig. 3. The ratio was calculated by dividing the integral intensity of YL by that of UVL, which were measured at the stage temperature of 200 K. In this study, energy ranges of YL and UVL were defined as 2.1–2.3 eV and 3.1–3.5 eV, respectively. The ratio tended to increase with P_{bias}. Cao *et al*. investigated the effects of Ar or H_2 plasma exposure on the electrical properties of p-type GaN films and reported that the concentration of shallow donor states induced by plasma exposure depended on ion energy[12]. Therefore, the trend suggests an increase in etching-induced damage, i.e., the total number of V_N, owing to high ion energies at a high P_{bias}.

Depth-resolved CL spectroscopy was carried out by measuring room-temperature CL intensity as a function of electron-beam penetration depth. The relationship between the penetration depth and E_b is roughly expressed as [27,28]

$$R_{KO} = \frac{0.0276A}{Z^{0.89}\rho} E_b^{1.67}, \quad (1)$$

where R_{KO} is the Kanaya–Okayama penetration depth (μm), A is the molecular weight (g/mol), Z is the average atomic number, ρ is the density (g/cm^3), and E_b is the electron-beam energy (keV). It has also been reported that the maximum CL generation depth approximated from a total primary electron energy-loss profile is about $0.3R_{KO}$[29,30]. To obtain depth-

resolved properties as changes in CL signal intensity, P_b was fixed at a low value of 12 μW[30]. The SEM scanning area was also fixed at 127×95 μm^2 in all the measurements. Fig. 4 shows the room-temperature CL spectra of the sample etched by ICP–RIE with P_{bias} of 15 W and E_b set at 3.0, 5.0, and 7.0 keV. Emission peaks in the UVL, BL, and YL bands similar to those in the PL spectra shown in Fig. 2(b) were observed, and the YL-to-UVL ratio of each peak depended on E_b. Fig. 5 shows the dependence of the YL-to-UVL ratio on E_b for the unetched sample and for the samples etched by ICP–RIE with P_{bias} of 2.5 and 15 W. The top horizontal axis shows the corresponding electron-beam penetration depth and maximum CL generation depth. Looking first at the signal for the sample etched by ICP–RIE with P_{bias} of 15 W, a relatively high YL-to-UVL ratio was observed at low energies, which dropped at E_b of 5.0–6.0 keV. This suggests that a high concentration of YL luminescence centers, i.e., isolated V_N, exists up to the maximum penetration depth of about 200 nm from the surface, and the concentration decreases rapidly at greater depths. Although the depth of damage depends on the plasma conditions, when considering the maximum CL generation depth, our value of $0.3R_{KO} \approx 60$ nm is of the same order of magnitude as that determined by wet etching and electrical methods in previous studies[12,22]. Note that a relatively high YL-to-UVL ratio observed at a high E_b (~10 keV) is due to the underlying Si-doped n-type GaN substrate[31]. On the other hand, for the sample etched by ICP–RIE with P_{bias} of 2.5 W, a ratio similar to that of the unetched sample was observed. This means that there are almost no etching-induced V_N at a penetration depth of more than 100 nm. Therefore, low-P_{bias} ICP–RIE with a low ion energy suppressed the introduction of etching-induced damage in the depth direction.

Finally, electrical contacts on the samples were evaluated by *I–V* measurements. Fig. 6 shows *I–V* characteristics of the unetched and etched samples. The *I–V* curves of the etched samples become closer to that of the unetched sample upon reducing P_{bias}. In particular, for the sample etched by ICP–RIE with P_{bias} of 2.5 W, the *I–V* characteristic is almost identical to that of the unetched sample. Fig. 7 shows intercept voltage (V_{int}) as a function of P_{bias}, and the inset shows the definition and extraction of V_{int} from an *I–V* curve[32]. V_{int} represents voltage drop in the damaged layer and is an indicator of ohmic characteristics[32]. V_{int} tended to increase with P_{bias}. Narita *et al.* investigated the surface band bending of an etched p-type GaN film by hard X-ray photoelectron spectroscopy and found that the thickness of a layer containing a high concentration of deep donors, which forms a hole barrier, increased with P_{bias}[33]. As mentioned previously, an emission peak in the YL band, which is likely caused by isolated V_N acting as a trivalent donor, was observed from the PL spectra of the etched samples, and

the results of depth-resolved CL spectroscopy suggest that V_N are introduced deeply with increasing P_{bias}. Therefore, it is assumed that the higher V_{int} at a higher P_{bias} results from the thickening of the hole barrier caused by the introduction of V_N to a greater depth.

4. Conclusions

We investigated the etching-induced damage in heavily Mg-doped p-type GaN. From low-temperature PL measurements, broad YL emission with a maximum at around 2.2–2.3 eV, which is likely caused by isolated V_N, was observed only in the etched samples. Depth-resolved CL spectroscopy based on room-temperature CL measurements revealed that the etching-induced YL was distributed up to the electron-beam penetration depth of around 200 nm at a high P_{bias}. Low-P_{bias} ICP–RIE was carried out with the aim of reducing damage, and it was found to reduce the YL-to-UVL ratio and its depth distribution to values similar to those of the unetched sample. Reducing P_{bias} could also improve the electrical characteristics; the I–V characteristic of the sample etched with P_{bias} of 2.5 W was comparable to that of the unetched sample. It is thus concluded that low-P_{bias} ICP–RIE is effective for suppressing etching-induced damage in heavily Mg-doped p-type GaN and improving the electrical properties of the etched surface.

Acknowledgments

This work was supported by the Ministry of the Environment “Project of Technical Innovation to Create a Future Ideal Society and Lifestyle”.

References

1) T. Oka, Y. Ueno, T. Ina, and K. Hasegawa, Appl. Phys. Express **7**, 021002 (2014).
2) T. Oka, T. Ina, Y. Ueno, and J. Nishii, Appl. Phys. Express **8**, 054101 (2015).
3) R. D. Dupuis, J. Kim, Y.-C. Lee, Z. Lochner, M.-H. Ji, T.-T. Kao, J.-H. Ryou, T. Detchphrom, and S.-C. Shen, ECS Trans. **58**, 261 (2013).
4) S.-C. Shen, R. D. Dupuis, Z. Lochner, Y.-C. Lee, T.-T. Kao, Y. Zhang, H.-J. Kim, and H.-H. Ryou, Semicond. Sci. Technol. **28**, 074025 (2013).
5) S. J. Pearton, R. J. Shul, and F. Ren, MRS Internet J. Nitride Semicond. Res. **5**, 11 (2000).
6) Z.-Q. Fang, D. C. Look, X.-L. Wang, J. Han, F. A. Khan, and I. Adesida, Appl. Phys. Lett. **82**, 1562 (2003).
7) S. Kim, Y. Hori, W.-C. Ma, D. Kikuta, T. Narita, H. Iguchi, T. Uesugi, T. Kachi, and T. Hashizume, Jpn. J. Appl. Phys. **51**, 060201 (2012).
8) R. J. Shul, L. Zhang, A. G. Baca, C. G. Willison, J. Han, S. J. Pearton, and F. Ren, J. Vac. Sci. Technol. A **18 (4)**, 1139 (2000).
9) N. Asai, H. Ohta, F. Horikiri, Y. Narita, T. Yoshida, and T. Mishima, Jpn. J. Appl. Phys. **58**, SCCD05 (2019).
10) R. Kometani, K. Ishikawa, K. Takeda, H. Kondo, M. Sekine, and M. Hori, Appl. Phys. Express **6**, 056201 (2013).
11) Z. Liu, J. Pan, A. Asano, K. Ishikawa, K. Takeda, H. Kondo, O. Oda, M. Sekine, and M. Hori, Jpn. J. Appl. Phys. **56**, 026502 (2017).
12) X. A. Cao, S. J. Pearton, A. P. Zhang, G. T. Dang, F. Ren, R. J. Shul, L. Zhang, R. Hickman, and J. M. Van Hove, Appl. Phys. Lett. **75**, 2569 (1999).
13) A. Baharin, M. Kocan, U. K. Mishra, G. Parish, and B. D. Nener, Opt. Mater. **32**, 700 (2010).
14) J.-M. Lee, K.-S. Lee, and S.-J. Park, J. Vac. Sci. Technol. B **22 (2)**, 479 (2004).
15) J.-M. Lee, K.-M. Chang, S.-W. Kim, C. Huh, I.-H. Lee, and S.-J. Park, J. Appl. Phys. **87**, 7667 (2000).
16) D. G. Kent, K. P. Lee, A. P. Zhang, B. Luo, M. E. Overberg, C. R. Abernathy, F. Ren, K. D. Mackenzie, S. J. Pearton, and Y. Nakagawa, Solid-State Electron. **45**, 1837 (2001).
17) K.-M. Chang, C.-C. Cheng, and J.-Y. Chu, J. Electrochem. Soc. **149**, G367 (2002).
18) Y.-T. Moon, D.-J. Kim, J.-S. Park, J.-T. Oh, J.-M. Lee, and S.-J. Park, J. Vac. Sci. Technol. B **22 (2)**, 489 (2004).
19) A. Terano, H. Imadate, and K. Shiojima, Materi. Sci. Semicond. Process. **70**, 92 (2017).
20) J. He, Y. Zhong, Y. Zhou, X. Guo, Y. Huang, J. Liu, M. Feng, Q. Sun, M. Ikeda, and H.

Yang, Appl. Phys. Express **12**, 055507 (2019).

21) M. Kato, K. Mikamo, M. Ichimura, M. Kanechika, O. Ishiguro, and T. Kachi, J. Appl. Phys. **103**, 093701 (2008).
22) S. Yamada, M. Omori, H. Sakurai, Y. Osada, R. Kamimura, T. Hashizume, J. Suda, and T. Kachi, Appl. Phys. Express **13**, 016505 (2020).
23) T. Kumabe, Y. Ando, H. Watanabe, Y. Honda, M. Deki, A. Tanaka, S. Nitta, and H. Amano, Ext. Abstr. Solid State Devices and Materials, 2020, p. 199.
24) W. Kern and D. A. Puotinen, RCA Rev. **31**, 187 (1970).
25) M. A. Reshchikov and H. Morkoç, J. Appl. Phys. **97**, 061301 (2005).
26) Q. Yan, A. Janotti, M. Scheffler, and C. G. Van de Walle, Appl. Phys. Lett. **100**, 142110 (2012).
27) K. Kanaya and S. Okayama, J. Phys. D: Appl. Phys. **5**, 43 (1972).
28) J. I. Goldstein, D. E. Newbury, D. C. Joy, C. E. Lyman, P. Echlin, E. Lifshin, L. Sawyer, and J. R. Michael, *Scanning Electron Microscopy and X-Ray Microanalysis 3rd edition* (Springer, New York, 2003) p. 72.
29) M. Toth and M. R. Phillips, Scanning **20**, 425 (1998).
30) K. Fleischer, T. Toth, M. R. Phillips, J. Zou, G. Li, and S. J. Chua, Appl. Phys. Lett. **74**, 1114 (1999).
31) I.-H. Lee, I.-H. Choi, C. R. Lee, and S. K. Noh, Appl. Phys. Lett. **71**, 1359 (1997).
32) T. Makimoto, K. Kumakura, and N. Kobayashi, J. Cryst. Growth **221**, 350 (2000).
33) T. Narita, D. Kikuta, N. Takahashi, K. Kataoka, Y. Kimoto, T. Uesugi, T. Kachi, and M. Sugimoto, Phys. Stat. Solidi A **208 (7)**, 1541 (2011).

Figure Captions

Fig. 1. Schematic process flow of surface etching and electrode formation.

Fig. 2. Low-temperature PL spectra of (a) unetched p-type GaN and (b) p-type GaN etched by ICP–RIE with P_{bias} of 15 W. The temperature of the sample stage was controlled in the range of 5–200 K.

Fig. 3. Dependence of YL-to-UVL ratio on P_{bias}. The ratio was calculated by dividing the integral intensity of YL (2.1–2.3 eV) by that of UVL (3.1–3.5 eV), which were measured at the stage temperature of 200 K.

Fig. 4. Room-temperature CL spectra of p-type GaN etched by ICP–RIE with P_{bias} of 15 W. E_b was set at 3.0, 5.0, and 7.0 keV and P_b was fixed at 12 μW.

Fig. 5. Dependence of YL-to-UVL ratio on E_b for unetched sample and samples etched by ICP–RIE with P_{bias} of 2.5 and 15 W. The top horizontal axis shows the corresponding electron-beam penetration depth and maximum CL generation depth.

Fig. 6. *I–V* characteristics of unetched and etched samples.

Fig. 7. Intercept voltage (V_{int}) as a function of P_{bias}. The inset shows the definition and extraction of V_{int} from an *I–V* curve[32].

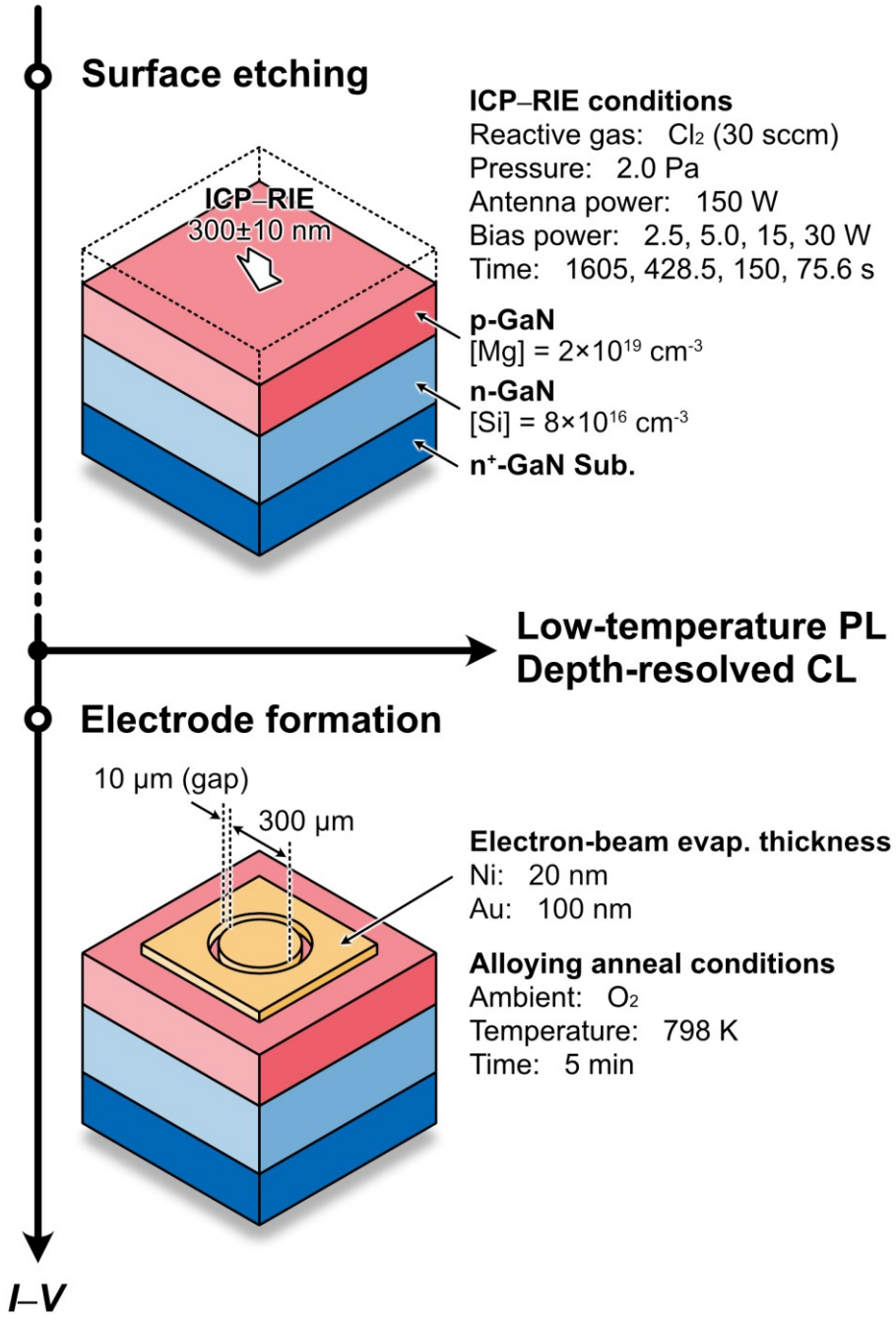
Surface etching
ICP–RIE conditions
Reactive gas: Cl2 (30 sccm)
Pressure: 2.0 Pa
Antenna power: 150 W
Bias power: 2.5, 5.0, 15, 30 W
Time: 1605, 428.5, 150, 75.6 s
ICP–RIE
300±10 nm
p-GaN
[Mg] = 2×10^19 cm^-3
n-GaN
[Si] = 8×10^16 cm^-3
n+-GaN Sub.
Low-temperature PL
Depth-resolved CL
Electrode formation
10 μm (gap)
300 μm
Electron-beam evap. thickness
Ni: 20 nm
Au: 100 nm
Alloying anneal conditions
Ambient: O2
Temperature: 798 K
Time: 5 min
I–V

Fig. 1

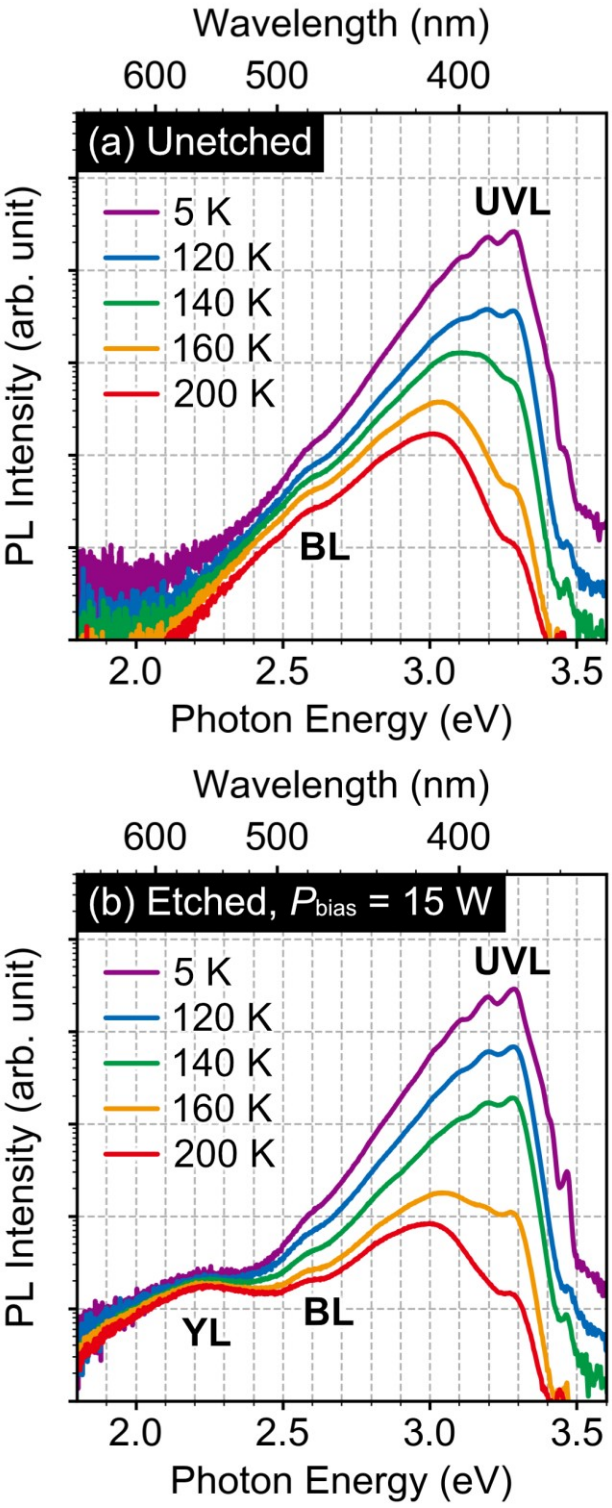
Wavelength (nm)
600
500
400
(a) Unetched
5 K
120 K
140 K
160 K
200 K
UVL
BL
PL Intensity (arb. unit)
2.0
2.5
3.0
3.5
Photon Energy (eV)
Wavelength (nm)
600
500
400
(b) Etched, P_{bias} = 15 W
5 K
120 K
140 K
160 K
200 K
UVL
YL
BL
PL Intensity (arb. unit)
2.0
2.5
3.0
3.5
Photon Energy (eV)

Fig. 2

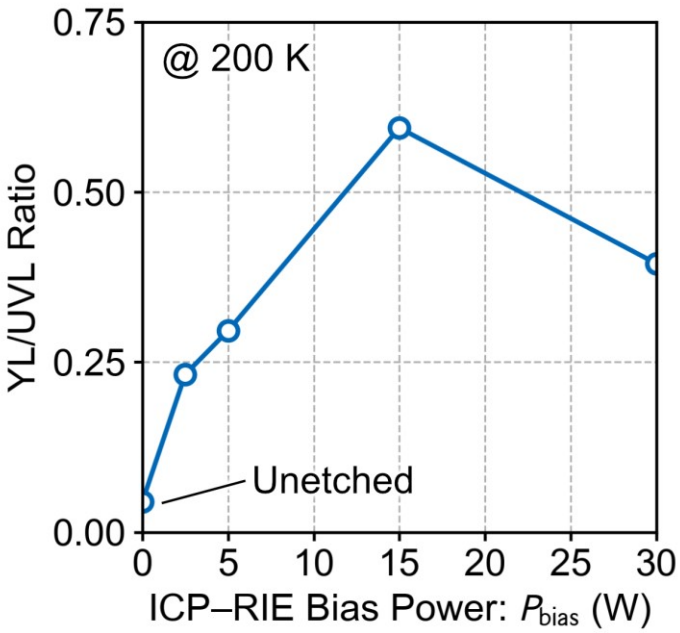
0.75
@ 200 K
0.50
YL/UVL Ratio
0.25
Unetched
0.00
0
5
10
15
20
25
30
ICP–RIE Bias Power: P_{bias} (W)

Fig. 3

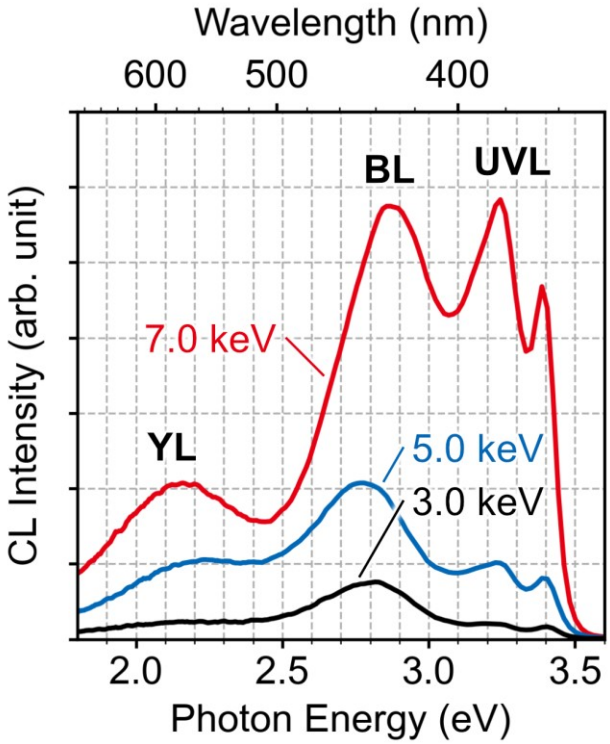
Wavelength (nm)
600
500
400
BL
UVL
7.0 keV
YL
5.0 keV
3.0 keV
CL Intensity (arb. unit)
2.0
2.5
3.0
3.5
Photon Energy (eV)

Fig. 4

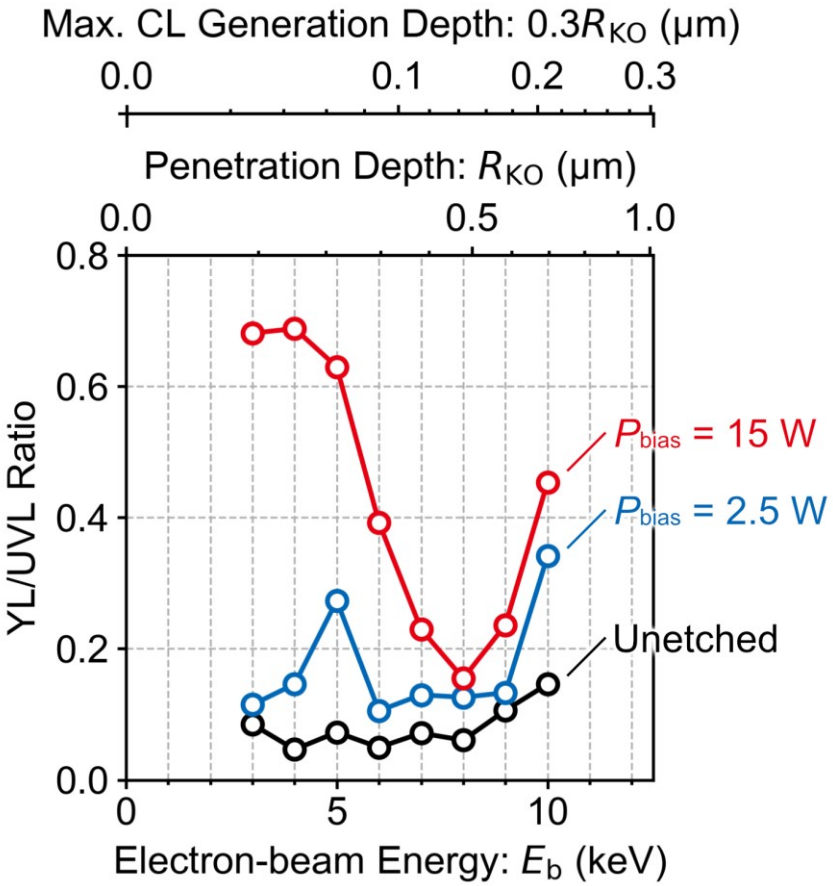
Max. CL Generation Depth: 0.3R_{KO} (μm)
0.0
0.1
0.2
0.3
Penetration Depth: R_{KO} (μm)
0.0
0.5
1.0
0.8
0.6
0.4
0.2
0.0
YL/UVL Ratio
P_{bias} = 15 W
P_{bias} = 2.5 W
Unetched
0
5
10
Electron-beam Energy: E_b (keV)

Fig. 5

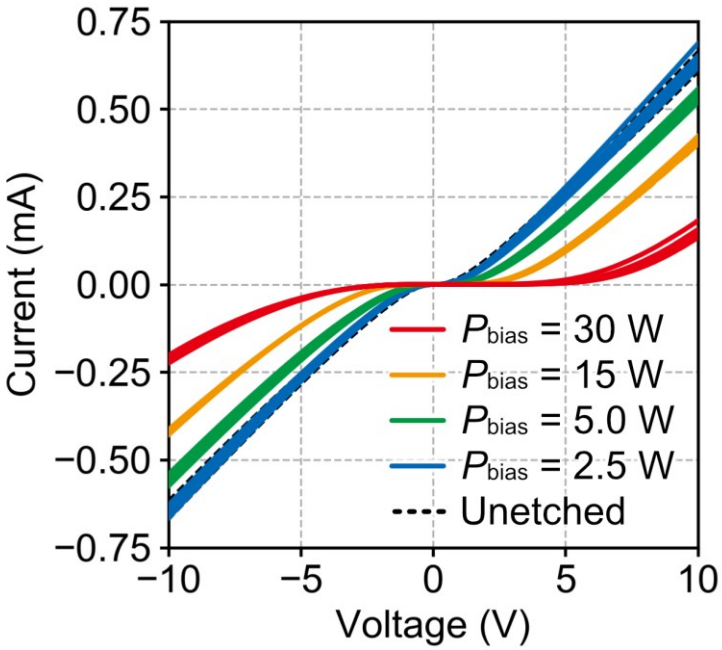
0.75
0.50
0.25
0.00
−0.25
−0.50
−0.75
Current (mA)
−10
−5
0
5
10
Voltage (V)
P_{bias} = 30 W
P_{bias} = 15 W
P_{bias} = 5.0 W
P_{bias} = 2.5 W
Unetched

Fig. 6

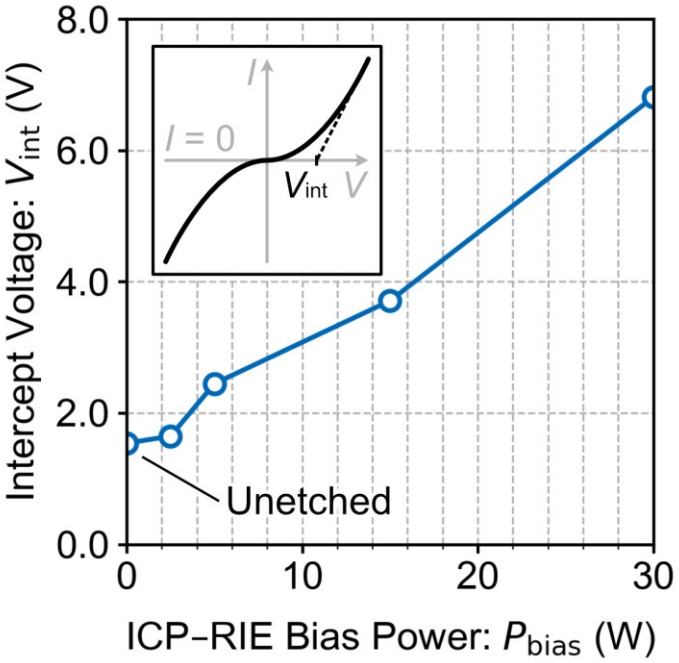
8.0
6.0
4.0
2.0
0.0
0
10
20
30
Intercept Voltage: V_{int} (V)
ICP–RIE Bias Power: P_{bias} (W)
Unetched
I
I = 0
V_{int}
V

Fig. 7